JPE 17-2-22

https://doi.org/10.6113/JPE.2017.17.2.542
ISSN(Print): 1598-2092 / ISSN(Online): 2093-4718

Research on the Power Sharing Control and Stability of VSGs

Dong Xie†, Da-Jin Zang*, Peng Gao*, and Jun-Jia Wang*

†,*Department of Electrical Engineering, Tongling University, Tongling, China

Abstract

Aiming at the deficiencies of power sharing control performances when a traditional droop control is adopted for microgrid inverters, this paper proposes a microgrid inverter power sharing control strategy based on a virtual synchronous generator. This control method simulates the electromechanical transient characteristics of a synchronous generator in a power system by an ontology algorithm and the control laws of a synchronous generator by control over the speed governor and excitation regulator. As a result, that the microgrid system is able to effectively retain the stability of the voltage and frequency, and the power sharing precision of the microgrid inverter is improved. Based on an analysis of stability of a microgrid system controlled by a virtual synchronous generator, design thoughts are provided for further improvement of the power sharing precision of inverters. The simulation results shows that when the virtual synchronous generator based control strategy was adopted, the power sharing performances of microgrid inverters are improved more obviously than those using the droop control strategy.

Key words: Microgrid, inverter, Power sharing control, Stability, Virtual synchronous generator

I. INTRODUCTION

Distributed generation (DG), with advantages such as reduced pollution, high reliability, high energy availability, flexible installation sites, etc, is an important development direction for future global energy technology. After a number of distributed power supplies are connected to the existing distribution networks, electric energy quality problems may be caused, such as deviations of the grid voltage and frequency, voltage fluctuation and so on, all of which seriously endanger the safe and reliable operation of the grid. In order to coordinate the conflicts between a large grid and distributed generation and to sufficiently explore the efficiencies of distributed power supplies, CERTS brought forward the concept of a microgrid in the beginning of this century [1]-[3].

Microgrids run jointly and switch to the islanding operation mode in the case of a grid failure so as to uninterruptedly supply power to critical loads. The key to the operation of a microgrid rests on control of the microgrid inverter, and microgrid inverters mainly achieve their coordinative control and accepts the unified control of a large-scale grid by droop control under the multi-inverter connected condition [4]. The disadvantage of the droop control depends on the voltage and frequency deviation in the steady state and the complex mode switchover. In the case of varied micro-sources and differences between the equivalent output impedance and the rated capacity of a microgrid inverter, the load power cannot be distributed proportionally according to the rated micro-source capacity. This results in a serious circular current of parallel inverters under the islanding operation mode and affects the safety and stability of the microgrid.

Due to the disadvantages of droop control reported in [5]-[6], improved droop control strategies have been proposed to improve the power sharing control performance of microgrid inverters. However, droop control can only reflect the external characteristics of a synchronous generator. It cannot achieve the characteristics of synchronous generators such as large inertia and large output inductance. A large inertia is conducive to the stability of the frequency of a microgrid system, and a large output inductance is advantageous in the control of inverters which are operated in the islanding mode. This shows that the synchronous generator characteristics are very conducive to the formation

Manuscript received Jun. 22, 2016; accepted Dec. 3, 2016
Recommended for publication by Associate Editor Kai Sun.
†Corresponding Author: XDY@tlu.edu.cn
Tel: +86-13305620183, Tongling University
*Department of Electrical Engineering, Tongling University, China

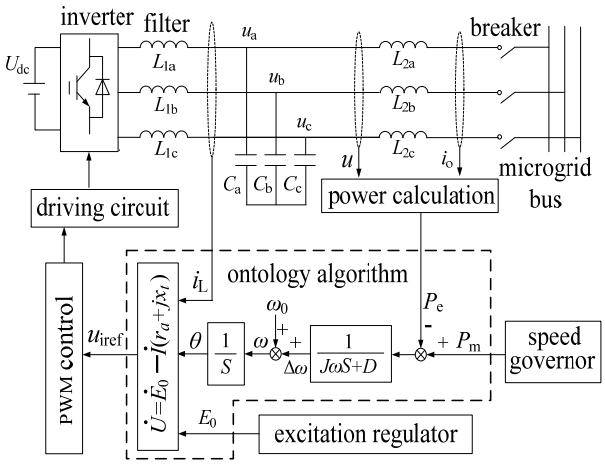

Fig. 1. Theory diagram of virtual synchronous generator.

of a microgrid, because microgrids are constructed using small inertia, low output impedance inverters.

To further improve the performance of the power sharing control of a microgrid inverter, a novel inverter control strategy was proposed based on the "virtual synchronous generator (VSG)" in [7]-[9]. This control strategy can show the excellent characteristics of a synchronous generator, and quickly follow up the dynamic change of the distribution network/microgrid so as to realize precise output power sharing of parallel inverters. This benefits the reliable operation of an inverter-typed power supply and improves the quality of electric energy. However, the above literature presents no specific design process for the active and reactive power sharing control when multiple microgrid inverters run jointly. Therefore, this paper proposes a specific analysis and computing methods for power sharing control among VSG control based inverters during the islanding operation mode. Additionally, the precision of VSG power sharing control can be improved by raising the stability of a microgrid system. Accordingly, this paper carries out detailed analyses on the VSG operating stability to provide some favorable references for the optimized design of a VSG and for further raising the VSG power sharing control performance. Finally, microgrid system simulation and experimental models composed by two VSG control based inverters are established. These simulation and experimental results demonstrate the effectiveness of the power sharing control methods proposed in this paper.

II. OPERATING PRINCIPE OF A VSG

The operating principle of a VSG control based microgrid inverter is as shown in Fig. 1.

In Fig. 1, the main circuit employs a three-phase voltage-typed inverter, where L_{1i} and C_i indicate the filter inductance and filter capacity (i=a, b, c), and L_{2i} is used as the external inductance to ensure that the output impedance is inductive and to realize the power control. By detecting the output current i_{oabc} flowing across L_{2i} and the output voltage u_{abc} on the two ends of the filter capacity C_i, the power calculation is performed to achieve the output power P_e of the inverter. Then the mechanical input power directive P_m and the excitation inductance electromotive force directive E_0 of the VSG are derived from the speed governor and excitation regulator. With P_e, P_m and E_0 derived and the inductive current i_{Labc} detected, the ontology algorithm of the VSG is used to calculate the voltage directive U_{iref} of the filter capacity C_i. Finally, the PWM control and driver circuit are used to control the power switch devices of the inverter so that the inverter is able to simulate the basic characteristics and control features of a synchronous generator.

The electromechanical transient mathematic model of the synchronous generator is composed of the rotor motion equation in formula (1) and the stator electrical equation in formula (2) as follows [10]-[11].

$$P_m - P_e - D\Delta\omega = J\omega\frac{d\Delta\omega}{dt} \tag{1}$$

$$\dot{U}_i = \dot{E}_{0i} - \dot{I}_i(r_a + jx_t) \tag{2}$$

P_m and P_e in formula (1) are the rotor mechanical input power and stator electromagnetic power of the synchronous generator, D indicates the damping coefficient, ω indicates the operating frequency of the synchronous generator, $\Delta\omega$ indicates the difference between the frequency's given value and the actual value, and J indicates the moment of inertia. E_{0i} and U_i in formula (2) show electromotive force of the excitation induction and terminal voltage in the i^{th} phase of the stator winding, I_i indicates the stator current, r_a and x_t indicate the armature resistance and synchronous reactance of the stators.

By simulating an electromechanical transient mathematic model of the synchronous generator by the ontology algorithm of the VSG, the microgrid inverter has characteristics similar to self-synchronization, a large output inductive reactance and a large moment of inertia of the synchronous generator, which are very favorable for restricting the current mutation and power control. The ontology algorithm structure of the VSG is specified in the lower dotted frame shown in Fig.1.

III. POWER SHARING CONTROL OF A VSG

Under the islanding operation mode, microgrid inverters stay in the state of parallel operation and the inverters control their output power according to their own capacities so that active and reactive loads are distributed reasonably among the parallel inverters [12].

A. Active Power Sharing Control of a VSG

The speed governor of a VSG is designed to meet the frequency stability of a microgrid system by simulating the

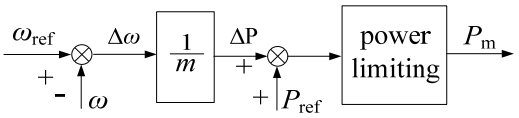

Fig. 2. Block diagram of VSG speed governor.

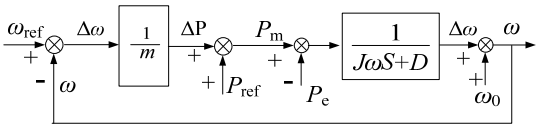

Fig. 3. The structure of VSG frequency closed loop control.

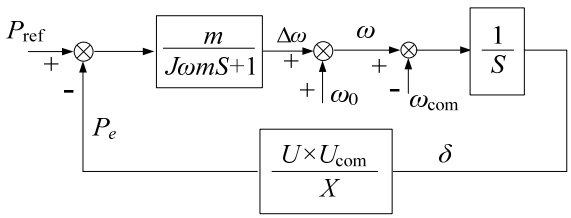

Fig. 4. The structure of VSG active power closed loop control.

power and frequency characteristics of the synchronous generator and realizing the sharing control of the inverter output active power [13]. The power-frequency characteristics of the synchronous generator are expressed as:

$$P_{\text{ref}} - P = -\frac{1}{m}(\omega_{\text{ref}} - \omega) \tag{3}$$

In this formula, P_{ref} and P indicate the given and actual values of the synchronous generator's output power, ω_{ref} and ω indicate the given and actual values of the synchronous generator operating frequency, m is named as the active power-frequency regulation coefficient, and the value of m indicates the mechanical input power variance of the synchronous generator during a frequency change. The smaller m is, the larger the mechanical input power variance becomes. The speed governor of the VSG needs to control the mechanical input power of the VSG, so that the VSG has the same power-frequency characteristics as the synchronous generator set, and the control structure of the VSG speed governor can be deduced by formula (3) as shown in Fig.2.

In order to realize the active power sharing control of the VSG, the regulation coefficient m_{k} and active capacity P_{k} of the VSG should meet the following relation:

$$m_1 P_1 = m_2 P_2 = ... = m_{\text{k}} P_{\text{k}} \tag{4}$$

The closed-loop frequency control structure of the VSG can be deduced as shown in Fig.3 according to the ontology algorithm of the VSG and speed governor control structure.

Considering that frequency directive ω_{ref} of the VSG is usually its reference frequency ω_0, the following transfer function expression can be deduced by Fig.3:

$$\frac{\omega - \omega_{\text{ref}}}{P_{\text{ref}} - P_{\text{e}}} = \frac{\Delta\omega}{\Delta P} = \frac{1}{J\omega S + D + 1/m} \tag{5}$$

Because the frequency modulation function of the speed governor is equivalent to increase the system damping, the damping coefficient D is assumed as 0, and formula (5) is simplified as:

$$\frac{\Delta\omega}{\Delta P} = \frac{m}{J\omega m S + 1} \tag{6}$$

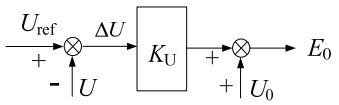

Fig. 5. Block diagram of VSG excitation controller.

If the equivalent output impedance of the VSG and the line impedance are inductive, the output active power of the VSG approximates to:

$$P_e = \frac{UU_{\text{com}}\delta}{X} \tag{7}$$

In this formula, U indicates the VSG output voltage, U_{com} indicates the parallel bus voltage of the inverter, δ indicates the angle difference (active angle) between the VSG output voltage and the parallel bus voltage, and X is the sum of the VSG equivalent output impedance and the line impedance.

The closed-loop active power control structure of the VSG can be deduced by the above analysis, as shown in Fig. 4.

The following is educed from Fig. 4.

$$P_e(s) = \frac{m\frac{UU_{\text{com}}}{X}}{J\omega m s^2 + s + m\frac{UU_{\text{com}}}{X}} \cdot P_{ref}(s) + \frac{(J\omega m s+1)\frac{UU_{\text{com}}}{X}}{J\omega m s^2 + s + m\frac{UU_{\text{com}}}{X}} \cdot [\omega_0(s) - \omega_{\text{com}}(s)] \tag{8}$$

According to formula (8), the output active power of the VSG at the steady state is as follows:

$$P_{\text{e}} = P_{\text{ref}} + \frac{1}{m} \cdot (\omega_0 - \omega_{\text{com}}) \tag{9}$$

Formula (9) indicates that parallel VSGs can share the active power of loads proportionally according to their capacities if the regulation coefficient m is set according to formula (4).

B. Reactive Power Sharing Control of the VSG

In power systems, the excitation control system of the synchronous generator set is used to automatically control the excitation voltage according to the deviation of the output voltage so that the excitation-induced electromotive force of the synchronous generator stator winding changes to maintain the voltage stability of the stator terminal under various load conditions and to realize the reactive power balance of the system [14]. In microgrid systems, the excitation regulator of the VSG maintains the output voltage stability and reactive power equilibrium of the inverters by simulating the excitation control system of the synchronous generator set. The control structure of the VSG excitation regulator can be educed, as shown in Fig. 5, according to the operating principle of the synchronous generator excitation control system.

In Fig. 5, U_{ref} and U denote the given value and actual value of the VSG output voltage, U_0 indicates rated value of the VSG stator voltage, E_{o} indicates the excitation-induced

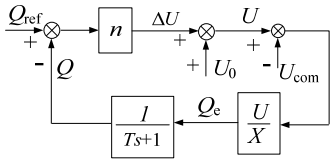

Fig. 6. The structure of VSG reactive power closed loop control.

electromotive force of the VSG stator, and K_u indicates voltage regulating coefficient of the VSG. In the case of the accurate setting of K_u, the VSG and synchronous generator have the same voltage regulating characteristics, to maintain the stability of the output voltage and public bus voltage and to control the reasonable distribution of the reactive power among parallel VSGs.

Under the islanding operation, in order to achieve the reactive power dispatch, the output voltage given value U_{ref} of the VSGs should satisfy the following formula in accordance with the VSG ontology algorithm and excitation regulator structure:

$$U_{ref} = U_0 + \frac{X_0}{3K_u U_0} Q_{ref} \tag{10}$$

In this formula, U_0 indicates the reference voltage of the VSG, X_0 indicates the equivalent output impedance of the VSG, K_u indicates the voltage regulating coefficient of the VSG, Q_{ref} indicates the output reactive power directive of the VSG. The VSG voltage regulating characteristic equation corresponding to formula (10) is as follows:

$$U - U_0 = -\frac{X_0}{3(1+K_u)U_0}(Q - Q_{ref}) = -n(Q - Q_{ref}) \tag{11}$$

In this formula, n shows the reactive power-voltage regulation coefficient of the VSG. In order to ensure that inverters share their reactive loads proportionally according to their capacities, the reactive power-voltage regulation coefficient n and reactive capacity Q_k of the VSGs need to meet the following:

$$n_1 Q_1 = n_2 Q_2 = ... = n_k Q_k \tag{12}$$

If the VSG equivalent output impedance and line impedance are inductive, the output reactive power of the VSG approximates the following:

$$Q = \frac{U(U - U_{COM})}{X} \tag{13}$$

The parameters in the formula above are the same as those in formula (7). The closed-loop reactive power control structure of the VSG is shown in Fig. 6.

The output reactive power of the VSG in the steady state is deduced from Fig.6:

$$Q_e = \frac{nU}{X + nU} \cdot Q_{ref} + \frac{U}{X + nU}(U_0 - U_{com}) \tag{14}$$

According to formula (14), the output reactive power of the VSG in the steady state are related to the VSG equivalent output impedance and line impedance. This is to ensure that the reactive power of the loads can be shared proportionally according to the capacities of the parallel VSGs. In addition,

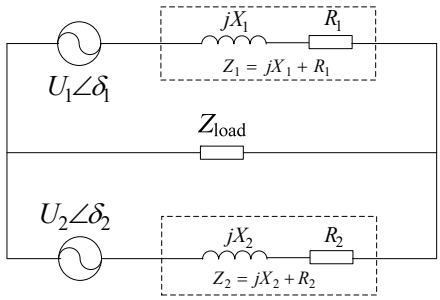

Fig. 7. Microgrid system equivalent circuit composed by two parallel VSGs.

by setting the reactive power-voltage regulating coefficient n according to formula (12), the following can be also met:

$$\frac{X_1}{n_1} = \frac{X_2}{n_2} = ... \frac{X_k}{n_k} \tag{15}$$

IV. Stability Analysis of a VSG

The power sharing control performance of a VSG is closely related to the stability of the VSG control based microgrid system. The virtual moment of inertia J and active-frequency regulation coefficient m are selected reasonably to achieve an optimized design of the VSG, to improve the stability of the microgrid system and to further raise the precision of the VSG power sharing control. The following carries out analyses on the stability of the VSG under the islanding operation mode.

Small-signal analysis is a common method for power system stability analysis, and it is used to analyze the dynamic behaviors of a system under the action of a small disturbance signal by establishing a small signal model of the system [15]. The equivalent circuit of a microgrid system composed by two parallel VSGs is shown in Fig. 7. Here Z_i(i=1, 2) is the sum of the VSG equivalent output impedance and the line impedance, U_i and δ_i are the output voltage and power angle of the two VSGs, and Z_{load} indicates a local load.

By the analysis in the previous section, it is known that the control characteristics of the active power-frequency and reactive power-voltage of the VSG are as follows:

$$\omega(s) = \omega_{ref}(s) + \frac{m}{J\omega m S + 1}[P_{ref}(s) - P_e(s)] \tag{16}$$

$$U(s) = U_0(s) - n[\frac{1}{Ts+1}Q_e(s) - Q_{ref}(s)] \tag{17}$$

In Fig. 7, if the steady state operating point of the two VSGs is (U_{i0}, δ_{i0}) (i=1, 2). At this point, the linearized time domain equation of the system is:

$$\begin{cases} \dfrac{d\Delta\delta_i}{dt} = \Delta\omega_i \\ \dfrac{d\Delta\omega_i}{dt} = \dfrac{1}{J_i\omega}(-\dfrac{1}{m_i}\Delta\omega_i - \Delta P_{ei}) \\ \Delta\dot{U}_i = \dfrac{1}{T_i}(-\Delta U_i - n_i\Delta Q_{ei}) \end{cases} \tag{18}$$

At the steady state operating point, the output active power and output reactive power of the VSGs can also be linearized, that is:

$$\begin{cases} \Delta P_{ei}(s)=\dfrac{\partial P_{ei}}{\partial U_1}\Delta U_1(s)+\dfrac{\partial P_{ei}}{\partial U_2}\Delta U_2(s) \\ \qquad\qquad +\dfrac{\partial P_{ei}}{\partial \delta_1}\Delta \delta_1(s)+\dfrac{\partial P_{ei}}{\partial \delta_2}\Delta \delta_2(s) \\ \Delta Q_{ei}(s)=\dfrac{\partial Q_{ei}}{\partial U_1}\Delta U_1(s)+\dfrac{\partial Q_{ei}}{\partial U_2}\Delta U_2(s) \\ \qquad\qquad +\dfrac{\partial Q_{ei}}{\partial \delta_1}\Delta \delta_1(s)+\dfrac{\partial Q_{ei}}{\partial \delta_2}\Delta \delta_2(s) \end{cases} \tag{19}$$

Setting $X=[\Delta\delta_1, \Delta\delta_2, \Delta\omega_1, \Delta\omega_2, \Delta U_1, \Delta U_2]^T$, according to (18) and (19), a small signal model of a VSG parallel network based microgrid system can be obtained as:

$$\dot{X}=AX \tag{20}$$

where:

$$A=\begin{bmatrix} 0 & 0 & 1 & 0 & 0 & 0 \\ 0 & 0 & 0 & 1 & 0 & 0 \\ -\dfrac{K_{11}}{J_1\omega_0} & -\dfrac{K_{12}}{J_1\omega_0} & -\dfrac{1}{J_1\omega_0 m_1} & 0 & -\dfrac{H_{11}}{J_1\omega_0} & -\dfrac{H_{12}}{J_1\omega_0} \\ -\dfrac{K_{21}}{J_2\omega_0} & -\dfrac{K_{22}}{J_2\omega_0} & 0 & -\dfrac{1}{J_2\omega_0 m_2} & -\dfrac{H_{21}}{J_2\omega_0} & -\dfrac{H_{22}}{J_2\omega_0} \\ -\dfrac{I_{11}n_1}{T_1} & -\dfrac{I_{12}n_1}{T_1} & 0 & 0 & -\dfrac{1+L_{11}n_1}{T_1} & -\dfrac{L_{12}n_1}{T_1} \\ -\dfrac{I_{21}n_2}{T_2} & -\dfrac{I_{22}n_2}{T_2} & 0 & 0 & -\dfrac{L_{21}n_2}{T_2} & -\dfrac{1+L_{22}n_2}{T_2} \end{bmatrix}$$

In matrix A:

$$K_{ij}=\frac{\partial P_{ei}}{\partial \delta_j}, H_{ij}=\frac{\partial P_{ei}}{\partial U_j}, I_{ij}=\frac{\partial Q_{ei}}{\partial \delta_j}, L_{ij}=\frac{\partial Q_{ei}}{\partial U_j} \text{ (i=1, 2; j=1, 2).}$$

The output active power and output reactive power of the two VSGs can be obtained from Fig. 7:

$$\begin{cases} P_{ei}=\dfrac{U_i^2}{|Z_{ii}|}\sin\alpha_{ii}+\dfrac{U_iU_j}{|Z_{ij}|}\sin(\delta_{ij}-\alpha_{ij}) \\ Q_{ei}=\dfrac{U_i^2}{|Z_{ii}|}\cos\alpha_{ii}+\dfrac{U_iU_j}{|Z_{ij}|}\cos(\delta_{ij}-\alpha_{ij}) \end{cases} \tag{21}$$

where:

$$\begin{cases} Z_{ii}=\dfrac{Z_1Z_2+(Z_1+Z_2)Z_{load}}{Z_i+Z_{load}}=R_{ii}+jX_{ii} \\ Z_{ij}=\dfrac{Z_1Z_2+(Z_1+Z_2)Z_{load}}{Z_{load}}=R_{ij}+jX_{ij} \end{cases},$$

$$\begin{cases} \alpha_{ii}=90^\circ-\arctan\dfrac{X_{ii}}{R_{ii}} \\ \alpha_{ij}=90^\circ-\arctan\dfrac{X_{ij}}{R_{ij}} \end{cases}$$

$\delta_{ij}=\delta_i-\delta_j$, (i=1,2; j=1,2; i≠j)。

Similarly, if (i=1, 2; j=1, 2; i≠j), by the above formulas, the corresponding coefficients in matrix A can be calculated as:

$$\begin{cases} K_{ii}=\dfrac{U_{i0}U_{j0}}{|Z_{ij}|}\cos(\delta_{ij0}-\alpha_{ij}) \\ K_{ij}=-\dfrac{U_{i0}U_{j0}}{|Z_{ij}|}\cos(\delta_{ij0}-\alpha_{ij})=-K_{ii} \end{cases} \tag{22}$$

$$\begin{cases} H_{ii}=\dfrac{2U_{i0}}{|Z_{ii}|}\sin\alpha_{ii}+\dfrac{U_{j0}}{|Z_{ij}|}\sin(\delta_{ij0}-\alpha_{ij}) \\ H_{ij}=-\dfrac{U_{i0}}{|Z_{ij}|}\sin(\delta_{ij0}-\alpha_{ij}) \end{cases} \tag{23}$$

$$\begin{cases} I_{ii}=\dfrac{U_{i0}U_{j0}}{|Z_{ij}|}\sin(\delta_{ij0}-\alpha_{ij}) \\ I_{ij}=-\dfrac{U_{i0}U_{j0}}{|Z_{ij}|}\sin(\delta_{ij0}-\alpha_{ij})=-I_{ii} \end{cases} \tag{24}$$

$$\begin{cases} L_{ii}=\dfrac{2U_{i0}}{|Z_{ii}|}\cos\alpha_{ii}-\dfrac{U_{j0}}{|Z_{ij}|}\cos(\delta_{ij0}-\alpha_{ij}) \\ L_{ij}=-\dfrac{U_{i0}}{|Z_{ij}|}\cos(\delta_{ij0}-\alpha_{ij}) \end{cases} \tag{25}$$

According to the Lyapunov small disturbance stability judgment principle, a system is stable if the real part of all of the eigenvalues of matrix A are negative. Accordingly, a small signal model and electrical control parameters during the VSG parallel operation are used to analyze the stability of the system by an analysis of the characteristic root track of matrix A. The electrical control parameters of the VSG during parallel operation are set as follows: the parameters of two VSGs are the same, namely the output impedance Z = (0.2+j2) Ω, the effective value of the VSG output voltage is 104V, given frequency value ω_{ref} = 314rad/s, the reactive power-voltage regulating coefficient n=0.001, the reactive filter time constant T=0.032s, and the load impedance Z_{load} =10Ω.

Fig. 8 indicates the characteristic root family of two VSG parallel network systems when taking different values of m and J, where the m values are 0.00157, 0.000314 and 0.000628 respectively and keep changeless, but J continuously changes from 0.1 to 10. From the root track curve, the damping and resonance frequency of the system are jointly dependent on m and J. In addition, the system has 6 poles, of which P_1 and P_2 are located changelessly. They are non-dominant acnodes because they are far away from the imaginary axis, and P_3 is located at the zero point without influencing the stability of the system. With an increase of J (arrow direction), P_4, P_5 and P_6 gradually change into a pair of conjugate complex roots from negative real roots and are dominant acnodes, and they decide the dynamic

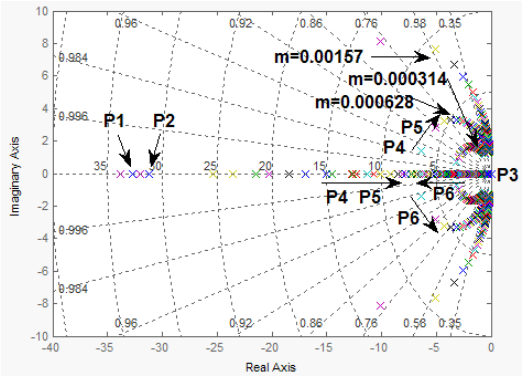

Fig. 8. Characteristic root family of two VSG parallel network systems

characteristics of the system. As shown in Fig.8, the larger the active frequency regulation coefficient m is, the more rapidly the dynamic response of the system can be configured. However, it is necessary to consider that the frequency in the steady state should not exceed the allowable change range. With an increase of J, the dynamic characteristics of the system accelerate gradually and then slow down and change from overdamping to underdamping. Therefore, the moment of inertia J should not be too small or large to ensure the stability of the system.

V. SIMULATION AND EXPERIMENTAL RESULTS OF THE VSG POWER SHARING CONTROL

In order to verify the control performance of the VSG based power sharing control strategy, a Matlab simulation model with two microgrid inverters as the VSG implement carrier was constructed.

The simulation parameters are set as follows: (1) the main circuit parameters: DC side voltage U_{dc}=400V, filter inductor L_1=1mH, filter capacitor C=30μF, additional line inductance L_2=0.5mH, the rated value of the system voltage amplitude and frequency are 311.127V and 314.1593rad/s; (2) the VSG ontology algorithm and controller parameters: the stator armature resistance is r_a=0Ω, the synchronous reactance is x_t=5mH, the moment of inertia is J=0.6kg*m^2, the damping coefficient is D=0, the active power-frequency regulation coefficients are m_1=10^{-4} and m_2=2×10^{-4}, the reactive power-voltage regulation coefficients are n_1=0.5×10^{-4} and n_2=10^{-4}, the active power given values are P_{ref1}=2000W and P_{ref2}=1000W, and the reactive power given values are Q_{ref1}= 1000Var and Q_{ref2}=500Var.

The simulation process is organized as follows: firstly the system is operated in the islanding mode. In the initial moment inverter 1 runs separately. The local loads are the active load 3000W and the inductive reactive load 1500Var. At 0.5 seconds, inverter 2 implements the pre-start control. The two inverters begin parallel operation when their output voltages meet the synchronization condition in the amplitude, phase and frequency, and jointly share the local load. At 2 seconds, the local loads have a mutation where the active load increases 1500W and the inductive reactive load increases 1500Var. The simulation results are shown in Fig. 9.

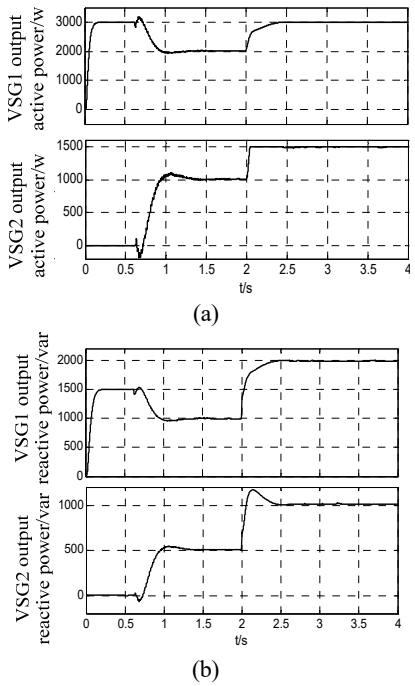

Fig. 9. The simulation waveforms of VSG control.

Fig. 9(a) shows simulation waveforms of the output active power of the two inverters. In the initial time, inverter 1 supplies 3000W for the local load separately, and the output power of inverter 2 is 0. At 0.7 seconds, inverter 2 is also put into operation through the pre-start control. Since their outputs for the active power are matched with the load, the two inverters output active power according to their given values. At 2 seconds, the active load suddenly increases 1500W. Since the active power-frequency regulation coefficients m_i of the two inverters are set according to formula (4), inverter 1 undertakes two-thirds of the new load while inverter 2 undertakes one-third of the new load. Therefore, the active power sharing control is achieved.

Fig.9(b) shows simulation waveforms of the output reactive power of the two inverters. Since the reactive power-voltage regulation coefficients of the two inverters are set to n_2=2n_1, from (12) it can be known that the reactive load undertaken by inverter 1 should be two times that of inverter 2. As can be seen from the waveform, the initial stage inverter 1 alone undertakes a 1500Var reactive load. After inverter 2 has been put into operation, the reactive load undertaken by inverter 1 is reduced from 1500Var to 1000Var, while inverter 2 undertakes a 500Var reactive load. This means that in the islanding mode, the output reactive power of the two inverters meets the requirements of the power sharing control. At 2 seconds, the reactive load suddenly increased by 1500 Var. After a very short transition

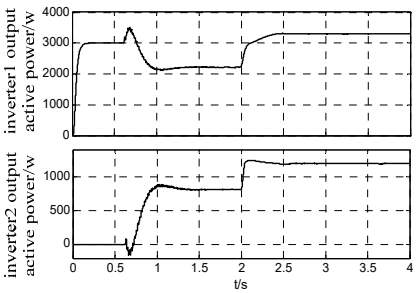

(a)

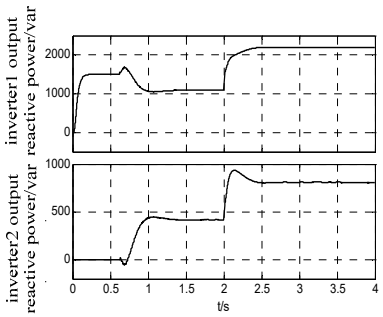

(b)

Fig. 10. The simulation waveforms of droop control.

time, the two inverters again undertake the reactive load according to the requirements of the reactive sharing control.

As control subjects, simulation waveforms of the power sharing control with the droop control are given in Fig. 10, where the parameter settings are the same as those of Fig. 9. As shown in Fig. 10(a), after inverter 2 is put into operation, the output active power of the two inverters have about 200W deviations, and the deviation will increase with an increase of the active load. From Fig. 10(b), it can be seen that the output reactive power of the two inverters also have deviation, and that they cannot accurately achieve power sharing control. A comparison of the simulation results shows that the power sharing control of the VSG-based control is significantly improved when compared to that of the droop control. This is due to its advantages in terms of a high output inductance and a large moment of inertia, as well as its simulation of the control characteristics of the synchronous generator in islanding mode, and the deviation of the inverter output active and reactive power is small.

In order to further validate the power sharing control effect of the VSG, an experimental system composed of two single phase inverters was set up. The main parameters of the system are as follows: the DC side voltage is 200V, the filter capacitor is 30μF, the filter inductance is 0.7mH, the line additional inductance is 0.5mH, the rated output voltage of the two inverters is 100V, inverter output terminals connect to the grid through a transformer, the active power-frequency regulation coefficients of the two VSGs are m_1= m_2=10^{-4}, and the reactive power-voltage regulation factors are both n_1= n_2=10^{-4}. Experimental verification waveforms are shown in Fig. 11.

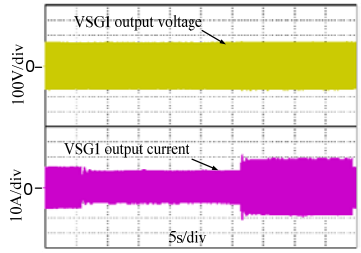

(a)

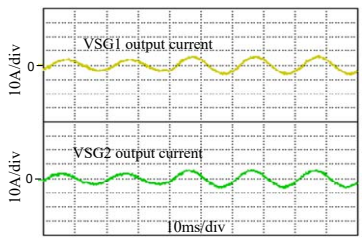

(b)

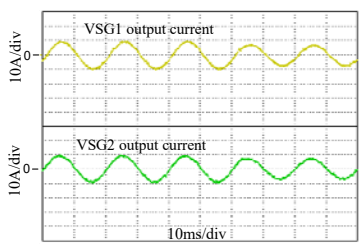

(c)

Fig.11. the experiment waveform of VSG control.

Fig. 11(a) shows experimental waveforms of the VSG mode switching and power scheduling after the grid connected operation. The selected load is 2000W/0Var. The island mode operation is first. Then the two VSGs operate in the grid connected mode after the synchronization requirement is achieved. They run for a period of time at a specified power of 1000W. Then the power specified values increase 500W and continue to run. Fig. 11(a) shows the output voltage and output current waveforms of VSG1, it shows that the VSG-based control strategy can meet the requirements of the inverter control, which can implement the operation mode switching and power scheduling.

Fig. 11(b) and Fig. 11(c) show load switching experimental waveforms for parallel VSGs which are operated in the island mode. In Fig. 11(b), the load at the moment from 700W/0Var suddenly increased to 1000W/0Var. The figure shows that the output current of the two VSGs increases dramatically with an increase of load and re-enters the steady state. At the same time, the output currents of the two VSGs are close to each other, indicating that the two VSGs have a fast dynamic response and good power sharing control characteristics. Fig. 11(c) shows experimental waveforms of a sudden decrease in the load from 1400W/0 Var to 1000W/0 Var at a certain moment. The figure also shows that the two VSGs have fast dynamic response characteristics and good power sharing control characteristics.

VI. CONCLUSIONS

The traditional droop control method has a large deviation in the power sharing control of microgrid inverters. Therefore, this paper proposes a novel VSG based microgrid inverter control technology. This control technology can achieve equilibrium distribution of the active and reactive load of a microgrid system due to the simulation of the electromechanical transient characteristics of a synchronous generator and the reference of the control principle of the synchronous generator speed governor and excitation regulator. In order to further improve power sharing control performance, a small signal analysis method is used to analyze the stability of the VSG control based a microgrid system, and it gives a reasonable choice of the control parameters m and J. Then it gives the VSG optimization design ideas to improve the accuracy of the power sharing control of a microgrid system. Simulation and experimental results has shown that the VSG can achieve a good power sharing, and its power sharing deviation is significantly smaller than that of the droop control based microgrid inverter.

ACKNOWLEDGMENT

This work is supported by the natural science foundation project of Anhui Province(160805ME120), the university natural science research project of Anhui Province (KJ2015A245), and Research Fund of Tongling University (2014tlxyrc03).

REFERENCES

[1] B. Meersman, J. M. Guerrero, and L. Vandevelde, "Voltage-based control of a smart transformer in a microgrid," *IEEE Trans. Ind. Electron*., Vol. 60, No. 4, pp.1291-1305, Apr. 2013.

[2] F. Nejabatkhah and Y.-W. Li, "Overview of power management strategies of hybrid AC/DC microgrid," *IEEE Trans. Power Electron*., Vol. 30, No. 12, pp. 7072-7089, Dec. 2015.

[3] M. Rasheduzzaman, J. A. Mueller, and J. W. Kimball, "Reduced-order small-signal model of microgrid systems," IEEE Trans. Sustain. Energy, Vol. 6, No. 4, pp. 1292-1305, Apr. 2015.

[4] X.-Q. Guo, Z.-G. Lu, B.-C. Wang, X.-F. Sun, L. Wang, and J. M. Guerrero, "Dynamic phasors-based modeling and stability analysis of droop-controlled inverters for microgrid applications," *IEEE Trans. Smart Grid*, Vol. 5, No. 6, pp. 2980-2987, Jun. 2014.

[5] J.-W. He and Y.-W. Li, "An enhanced microgrid load demand sharing strategy," *IEEE Trans. Power Electron*., Vol. 27, No. 9, pp. 3984-3995, Sep. 2012.

[6] W. Yao, M. Chen, J. Matas, J. M. Guerrero, and Z.-M. Qian, "Design and analysis of the droop control method for parallel inverters considering the impact of the complex impedance on the power sharing," *IEEE Trans. Ind. Electron*., Vol. 58, No. 2, pp. 576-588, Feb. 2011.

[7] J. Driesen, K. Visscher. "Virtual synchronous generators," *Proc. of the IEEE PES Meeting*, pp. 1-3, 2008.

[8] R. Aouini, K. B. Kilani, B. Marinescu, and M. Elleuch, "Virtual synchronous generators dynamic performances," *International Conference on Electrical Sciences and Technologies*, pp. 1-6, 2014.

[9] T. Shintai, Y. Miura, and T. Ise, "Oscillation damping of a distributed generator using a virtual synchronous generator," *IEEE Trans. Power Del*., Vol. 29, No. 2, pp. 668-676, Feb. 2014.

[10] C. N. Kawkabani and A. Schwery, "Modeling and control of large salient-pole synchronoushydro generators and stability issues in isolated production mode," *IEEE Workshop on Electrical Machines Design Control and Diagnosis*, pp. 148-157, 2013.

[11] M. Cisneros-González, C. Hernandez, R. Morales-Caporal, E. Bonilla-Huerta, and M. A. Arjona, "Parameter estimation of a synchronous generator two-axis model based on the standstill chirp test," *IEEE Trans. Energy Convers*., Vol. 28, No.1, pp. 44-51, Jan. 2013.

[12] G.-Q. Ding, F. Gao, Q.-R. Hao, and S. Zhang, "An improved power sharing control scheme of distributed generation converters in microgrid," *International Power Electronics and Application Conference and Exposition*, pp. 372-377, 2014.

[13] R. E. Cosse, M. D. Alford, M. Hajiaghajani, and E. R. Hamilton, "Fundamentals of turbine/generator speed control: a graphical approach for islanding applications," *IEEE Industry Applications Magazine*, Vol. 19, No. 4, pp. 56-62, Apr. 2013.

[14] R. Ramya, K. Selvi, and S. S. Nivethitha, "Optimization of synchronous generator excitation controller parameters," *International Conference on Power, Energy and Control*, pp. 585-590, 2013.

[15] H. Huang, C. Mao, J. Lu, and D. Wang, "Small-signal modelling and analysis of wind turbine with direct drive permanent magnet synchronous generator connected to power grid," *IET Renewable Power Generation*, Vol. 6, No. 1, pp. 48-58, Jan. 2012.

Dong Xie was born in Tongling, China. He received his M.S. and Ph.D. degrees in Electrical Engineering from the Hefei University of Technology, Hefei, China, in 2005 and 2014, respectively. From 1990 to 2000, he worked as an Engineer at the Tongling Vehicle Factory, Tongling, China. In 2000, he joined Tongling University, Tongling, China, where he is presently working as an Assistant Professor in the Department of Electrical Engineering. His current research interests include new energy and distributed generation technology, power system protection, and applications of embedded systems.

Da-Jin Zhang was born in China. He received his M.S. and Ph.D. degrees in Electrical Engineering from the China University of Mining and Technology, Xuzhou, China, in 1995 and 2007, respectively. From 1995 to 2000, he worked as an Engineer at the Taizhou Branch of the Agricultural Bank, Taizhou, China. From 2000 to 2007, he worked at Taizhou Polytechnic College, Taizhou, China, as an Assistant Professor. In 2007, he joined Tongling University, Tongling, China, where he is presently working as an Assistant Professor in the Department of Electrical Engineering. His current research interests include new energy and distributed generation technology, and intelligent signal processing.

Peng Gao was born in China. He received his M.S. degree in Power Electronics from the Anhui University of Technology, Maanshan, China, in 2010. He is presently working as a Lecturer in the Department of Electrical Engineering, Tongling University, Tongling, China, where he is teaching courses on power electronic technology and power system automation. His current research interests include power electronic technology and distributed generation technology.

Jun-Jia Wang was born in China. She received her M.S. degree in Electrical Theory and New Technology from the Institute of Plasma Physics, Chinese Academy of Sciences, Hefei, China, in 2010. She is presently working as a Lecturer in the Department of Electrical Engineering, Tongling University, Tongling, China, where she is teaching courses on power electronic technology. Her current research interests include power electronic technology and distributed generation technology.